scientific reports

OPEN

The effect of the displacement pressure on migration of fluid during the imbibition for tight oil reservoir

Yubin Yang[1], Xian Peng[1], Wenlian Xiao[2✉], Qihong Lei[3], Tao Li[1], Youan He[3], Chun Zhang[1], Jiahao Jiang[2], Tao Qi[1], Lingli Zheng[2] & Haoyu Chen[2]

In recent years, tight oil has emerged as a significant and complex topic in the fields of oil exploration and development. Following hydraulic fracturing, wells are typically shut-in for a designated period to facilitate water uptake into shale formations, which has become the predominant method for developing tight oil resources. During this process, initial pressure—specifically the shut-in pressure post-fracturing—plays a crucial role in ensuring imbibition recovery and determining shut-in duration. This study focuses on the typical terrestrial tight oil found in China—the Chang 7 tight oil from the Ordos Basin. Through quantitative analysis of wettability and pore-throat structure, we elucidate the flow mechanisms of oil during "shut-in" processes under varying pressure differentials using experiments conducted with nuclear magnetic resonance (NMR). Furthermore, we establish a model to quantitatively analyze the relationship between shut-in time and pressure across different reservoir types. Significant variations in wettability were observed among distinct pore spaces. Water-wet pores predominantly occurred within both small and large pores, whereas oil-wet pores were mainly identified in medium-sized pores. During imbibition, fluids initially mobilize crude oil within macropores with an impressive recovery rate reaching up to 25%. This process subsequently transitions into spontaneous sorption dynamics as infiltration continues, leading to reduced recovery rates primarily associated with micropores. Additionally, our findings indicate that the impact of shut-in pressure on enhanced imbibition recovery varies across different reservoir types. When the reservoir physical properties are better (i.e. the micro-fractures are more developed in the reservoirs), higher shut-in pressures correlate with improved imbibition recovery; optimal pressures are determined to be approximately 45 MPa ~ 55 MPa, with corresponding ideal shut-in durations of around 20 ~ 30 days. Conversely, the worse the reservoir physical properties are, we recommended to maintain maximum possible pressures to minimize shutdown periods while reducing ineffective downtime during well operations.

Keywords Tight oil, Wettability, Force imbibition, Shut-in time, Influence factor

Globally, conventional oil reservoirs have undergone a rapid and sustained decline, necessitating the urgent exploration of unconventional resources to mitigate global shortages[1–3]. Over the past decade, there has been a marked increase in oil production from unconventional reservoirs, particularly tight oil, which has positioned the United States and Canada as leading exporters of this hydrocarbon type[4–7]. Furthermore, large-scale development initiatives have been initiated in China, notably exemplified by the Chang 7 tight oil reservoir[8]. Consequently, the formulation of effective strategies for exploiting these unconventional resources has become a critical priority.

Hydraulic fracturing, which involves injecting substantial volumes of fracturing fluid to create complex fracture networks, has emerged as a prevalent technique for the extraction of tight oil. Following fracturing operations, immediate recovery of the fracturing fluid is not feasible; instead, it is standard practice to shut in the well for a period to allow the fracturing fluid to be absorbed into the formation and subsequently replaced by crude oil[9,10,][11–14]. During this process, imbibition serves as a critical mechanism for fluid exchange and enhanced

[1]Petro China Southwest Oil and Gas Field Branch, Chengdu, Sichuan, China. [2]State Key Laboratory of Oil and Gas Reservoir Geology and Exploitation, Southwest Petroleum University, Chengdu, Sichuan, China. [3]Petro China Changqing Oilfield Company, Xi'an, Shanxi, China. ✉email: joshxiao@163.com

oil recovery. Imbibition can generally be classified as either spontaneous or forced, depending on whether capillary pressure alone or an additional force drives the imbibition of fluid[15–18]. After hydraulic fracturing, the pressure within the fractures exceeds that of the matrix, causing a portion of the fracturing fluid to gradually flow into the matrix due to this pressure differential. Simultaneously, owing to the mixed-wettability characteristics of shale oil reservoir rocks, some of the fracturing fluid displaces crude oil from hydrophilic pores through capillary imbibition. Consequently, post-fracturing imbibition falls under the category of forced imbibition, occurring under the combined influence of pressure differential and capillary pressure ($P_c = 2\sigma\cos\theta/r$, σ is the interfacial tension, N/m, θ is the contact angle, ° ; r is the radius, μm). Therefore, both the pressure differential and microscopic pore-throat parameters play a crucial role in enhancing imbibition recovery efficiency, thereby influencing the determination of optimal shut-in time. Wang et al.[15] analyzed differences in flow dynamics between forced imbibition and spontaneous imbibition and found that oil recovery during forced imbibition was more than twice that observed during spontaneous imbibition for identical samples[16]. investigate the impact of reservoir properties on imbibition recovery. They findings indicated that the imbibition of the matrix system in rock samples play a critical role, particularly noting that pores larger than sub-micron in diameter contribute significantly to the imbibition recovery[19]. investigated the distribution of oil in pore throats during forced imbibition for four rocks with water wettability using nuclear magnetic resonance technology (NMR), identifying that during forced imbibition, most of the oil originates from pore throats larger than 100 μm[20]. conducted extensive spontaneous imbibition experiments using nuclear magnetic resonance (NMR) technology and found that the microscopic pore-throat structure parameters of rock samples are significant factors influencing their imbibition characteristics. Specifically, they observed a strong negative correlation between the average pore-throat ratio and the imbibition recovery, while the number of pores exhibited a positive correlation with the imbibition recovery[14]. conducted experimental research on mechanisms governing forced imbibition under shut-in conditions using X-ray computed tomography (X-CT) scanning techniques. They concluded that optimal shut-in time corresponds to the transition period from forced imbibition to spontaneous imbibition and developed a theoretical framework for calculating ideal shut-in durations[21]. investigated the fluid flow in oil–water–rock systems under the influence of spontaneous imbibition. Their findings suggest that the pore structure of core samples plays a crucial role in determining fluid flow within rock pores, indicating that the impact of spontaneous imbibition on oil recovery varies among different pore types. Even though the effect of the reservoirs on spontaneous imbibition at tight oil recovery has been explored at the pore-scale, the influence of pressure differential on spontaneous imbibition on tight oil recovery is still unclear, and the quantitative relationship between shut-in pressure and optimal shut-in times for different reservoir types has yet to be established.

In this study, we selected tight oil rock samples from adjacent locations to ensure that these samples exhibited very similar physical characteristics. We then characterized the pore throat spaces and analyzed the role of displacement pressure differences during imbibition using Nuclear Magnetic Resonance (NMR) technology. Based on these findings, we conducted numerical simulations by constructing various types of reservoirs and quantitatively analyzed their imbibition features under different shut-in pressures. Furthermore, we established a relationship between shut-in pressure and shut-in time for different types of reservoirs. This study provides a foundation for formulating an effective production system for tight oil reservoirs.

Materials and techniques
Materials
We prepared four cylindrical plugs, each with a diameter of 2.5 cm and an approximate length of 8 cm, from tight oil cores sourced from the Triassic Yangchang Formation in the Ordos Basin, located in northern China. The samples were cleaned of cutting oil using methylbenzene and a Soxhlet extractor, followed by drying at 85 °C for approximately 48 h. Prior to conducting experiments, their basic physical properties (Table 1) were determined. The porosity and gas permeability were measured under a confining pressure of 3 MPa (GB/T 29,172–2012). Each plug was subsequently divided into three sections: one section, approximately 4.0 cm in length, was used for dynamic imbibition tests; two sections, each approximately 2.0 cm long, were employed for Amott imbibition tests to evaluate wettability; while the remaining portion was reserved for CT scanning to characterize the pore structure.

Experimental procedures
Estimating the fluid distribution in pores of different sizes from NMR measurements
Low-field nuclear magnetic resonance (NMR), as an efficient, non-destructive and rapid technique for measuring fluids and their distribution, has been widely applied in core analysis. The primary application of NMR involves investigating the distribution of hydrogen-containing fluids within porous media[22]. The transverse relaxation

Sample	Length (cm)	Diameter (cm)	Porosity (%)	Permeability (mD)	Inlet pressure (MPa)	Outlet pressure(MPa)
1#	8.180	2.520	8.377	0.122	0	0.01
2#	8.180	2.510	7.150	0.096	1	0.01
3#	8.180	2.530	8.770	0.111	3	0.01
4#	8.150	2.540	8.430	0.127	6	0.01

Table 1. Basic physical properties and experimental arrangements of experimental rock samples.

time, T_2, of a fluid in a pore is composed of three parts: surface relaxation time (T_{2S}), bulk relaxation time (T_{2B}), and diffusion relaxation time (T_{2D})

$$\frac{1}{T_2} = \frac{1}{T_{2B}} + \frac{1}{T_{2S}} + \frac{1}{T_{2D}} = \frac{1}{T_{2B}} + \rho_2 \frac{S}{V} + \frac{D_f \left(\gamma G T_E\right)^2}{12} \tag{1}$$

where T_{2B} is the bulk relaxation time (ms), T_{2S} the surface relaxation time (ms), T_{2D} the diffusion relaxation time (ms), ρ_2 the surface relaxation strength ($\mu m/ms$), S the interstitial surface area (μm^2), V the pore-throat volume (μm^3), D_f the bulk diffusion coefficient of the pore fluid ($\mu m^2/ms$), γ the gyromagnetic ratio (MHz/T), G the gradient of the magnetic field (G/μm) and T_E the echo spacing time (ms). In general, the first and third terms on the right-hand side of Eq. (1) can be neglected in a magnetic field with a uniform gradient. This is because T_{2B} is significantly greater than T_{2S} (2–3 s), and the echo period (T_E) is chosen to be sufficiently short. Consequently, Eq. (2) can be simplified as follows:

$$\frac{1}{T_2} = \frac{1}{T_{2S}} = \rho_2 \frac{S}{V} \tag{2}$$

Meanwhile, the ratio of the interstitial surface area (S) to the volume (V) of rock pore throats can generally be expressed as the ratio of the pore throat shape factor (F_r) to the pore throat radius (r). Consequently, Eq. (3) can be rewritten as:

$$T_2 = \frac{1}{\rho_2} \frac{V}{S} = \frac{1}{\rho_2 F_r} r \tag{3}$$

Generally, both the surface relaxation rate and the pore throat shape factor can be regarded as approximately constant for the tight sandstone sample[22]. Consequently, there exists a one-to-one correspondence between the transverse relaxation time of the pore throat and its radius., i.e. the T_2 is proportional to r[23–27].

$$T_2 = Cr \tag{4}$$

Consequently, if the conversion coefficient C is known, the transverse relaxation time T_2 can be directly converted into the radius r of the pores occupied by the fluid of interest.

Wettability of samples
The Amott wettability index method is a fundamental approach employed for evaluating the wettability of rocks. This method determines rock wettability by comparing the water wettability index and the oil wettability index, which can be derived from Eqs. 5 and 6. The water wettability index and the oil wettability index represent, respectively, the degree of wetness of rocks in contact with water and crude oil. A higher water wettability index relative to the oil wettability index indicates that the rock has a greater propensity to be displaced by water, thus signifying"water wetting"; conversely, it reflects"oil wetting."[28–30]

$$Ww = \frac{\Delta V_{ws}}{\Delta V_{ws} + \Delta V_{wf}} \tag{5}$$

$$W_o = \frac{\Delta V_{os}}{\Delta V_{os} + \Delta V_{of}} \tag{6}$$

where W_w is water wettability index; W_o is oil wettability index; ΔV_{ws} is the oil production during the spontaneous imbibition water; ΔV_{wf} is the oil production during the waterflooding; ΔV_{os} is the water production during the spontaneous imbibition oil;ΔV_{of} is the oil production during the oilflooding. The Amott wettability index tests were conducted follow the SY/T 5153–2007 Standard of China. The heavy water was used as experimental water to shield the water-phase NMR signal. The simulated formation oil was a mixture of one volume of 5# while mineral oil for ten volumes of kerosene. At 20℃, this oil mixture has a viscosity of 1.5 mPa·s and a density of 0.85 g/cm³. The experiments were performed at room temperature (20 °C) following these specific steps: Samples were subjected to vacuum-pressurized saturation with heavy water, followed by simulated oil flooding to establish irreducible water saturation. Subsequently, the samples were aged at reservoir temperature for 15 days, and then the NMR T_2 spectrum were measured using a low-field NMR core analysis unit operating at a magnetic field strength of 0.5 T and hydrogen proton resonance frequency of 21.3 MHz. We employed the Carr–Purcell–Meiboom–Gill (CPMG) pulse sequence while setting waiting time (TW), echo spacing time (TE), number of echoes (NECH), and scanning number (NS) to values of 5000 ms, 0.5 ms, 18,000, and 32 respectively. ②The spontaneous imbibition apparatus was filled with heavy water, where the aged core samples underwent spontaneous water imbibition-oil expulsion experiments. The process was terminated when the oil displacement volume remained stable (<0.01 mL variation) for 24 consecutive hours. The spontaneous oil displacement volume (ΔV_{ws}) was recorded and NMR T2 spectra were acquired.③Heavy water flooding was performed on post-imbibition cores until the water cut at the outlet reached 99.95%. The water flooding oil displacement volume (ΔV_{wf}) and corresponding T2 spectra were documented.④ For oil spontaneous imbibition experiments, the water-flooded cores were immersed in simulated oil within the imbibition cell. The water expulsion process continued until stabilization (<0.01 mL variation). The spontaneous water expulsion volume (ΔV_{os}) and associated T2 spectra were measured.⑤ simulated oil flooding was implemented until achieving

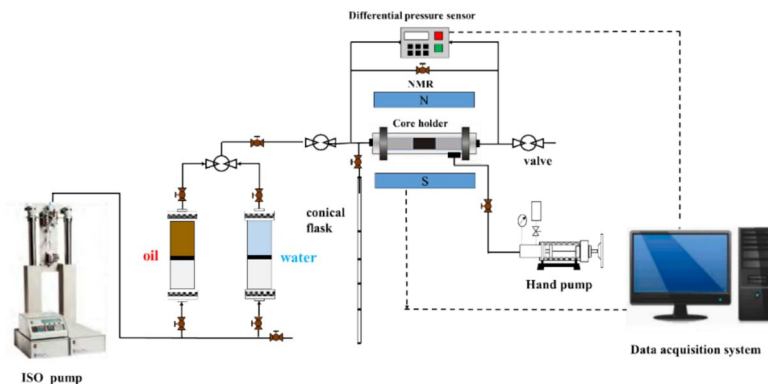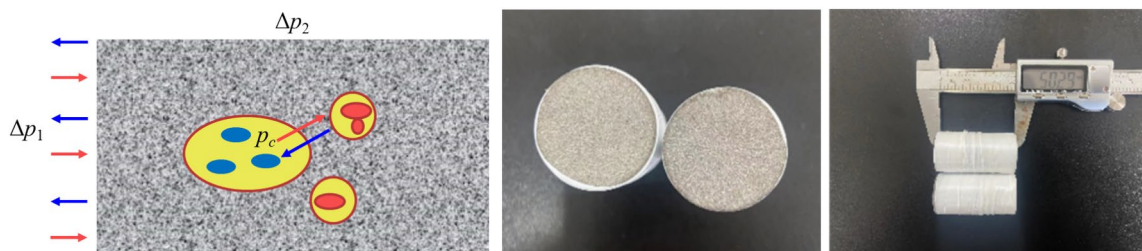**Fig. 1**. Experimental setup flowchart.

Fig. 2. Experimental rock samples.

99.95% oil content at the outlet. The oil flooding water displacement volume (ΔV_{of}) and corresponding T2 spectral data were recorded.

Forced imbibition
Forced imbibition tests were conducted on the remaining portions of the samples. As illustrated in Fig. 1, the experimental apparatus primarily comprised a high-pressure displacement pump, two cylinders for storing experimental pore water and simulated formation oil, a core holder, a hand pump for applying confining pressure, a nuclear magnetic resonance (NMR) system for real-time monitoring of fluid distribution, and a fluid collector. Meanwhile, the fluid in the fracture enters the formation and displaces crude oil into the fracture under the effect of the difference pressure and capillary pressure after hydraulic fracturing. Therefore, we used waterstop to seal three sides of the rock sample, leaving only one side in contact with the fluid to simulate the process of the fluid in the fracture entering the formation to replace crude oil (Fig. 2). During the experiment, the heavy water was used as experimental water to shield the water-phase NMR signal. The simulated formation oil was a mixture of one volume of 5# while mineral oil for ten volumes of kerosene. At 20℃, this oil mixture has a viscosity of 1.5 mPa·s and a density of 0.85 g/cm³.

The experiments were performed at room temperature (20 ℃) following these specific steps:

(1) The unjacketed samples were placed in a pressure vessel where they underwent vacuum treatment and saturation with experimental water at 20 MPa for over 48 h.
(2) The fully saturated samples were then loaded into the core holder and subjected to a confining pressure of 5 MPa. After verifying that there was no leakage, water was displaced from the sample by injecting simulated degassed crude oil at an injection pressure of 0.6 MPa until irreducible water saturation was achieved. Subsequently, the samples were aged at formation temperature for one week. Following aging, NMR T2 spectra of the samples.
(3) The plug was inserted in the outlet end of each rock sample to prevent any expulsion of crude oil from this end; heavy water was injected until reaching the pressure designated experimental.
(4) Once closed off from external flow by sealing the valve on the displacement pump, forced imbibition commenced. Real-time monitoring continued on NMR T_2 spectra until no further oil production occurred during this phase.

Result
Estimation of the conversion coefficients
NMR T_2 spectra capture the responses from both pores and throats. It is evident that the longest relaxation times are associated with the largest pores, as throats act as constrictions connecting these pores. Therefore, the

conversion coefficient C can be estimated as the ratio of $T_{2,max}$—the maximum measurable relaxation time—to the largest pore radius identified in CT scan images(Fig. 3).

For sample 1#, we determined a conversion coefficient of $C = 3.02$ ms/μm. Given that these samples were collected from adjacent locations, it is reasonable to assume they exhibit similar pore-throat distributions; therefore, this conversion coefficient can also be applied to all other samples. Furthermore, three categories of pores—micro-, meso-, and macropores—were defined based on specific ranges of pore throat radii: micropores for radii less than 0.1 μm, mesopores for radii ranging from 0.1 to 1 μm, and macropores for radii greater than 1 μm[22]. In our analysis of all the samples, the pore radius predominantly varied between 0.10 and 15.00 μm (Fig. 3), with an average radius of approximately 2 μm. The analysis indicated that micropores and mesopores account for significant proportions of the pore throat volume, comprising approximately 38% and 33%, respectively; in contrast, the development of macropores is relatively limited at only 29%.

NMR T_2 spectra of the amott wettability tests samples

In Figure 4, we present a comparison of the NMR T_2 spectrum for samples subjected to the Amott wettability test. The NMR T_2 spectrum predominantly reflects the oil signal, as heavy water was utilized as the experimental fluid. In all samples examined, the shape of the T_2 spectra exhibited variations, indicating a proportional change in T_2 amplitudes for relaxation times shorter than 1000 ms. Our findings reveal that both spontaneous imbibition of water and oil can occur within pore spaces corresponding to T_2 times less than 100 ms. This observation suggests that this portion of the pore space comprises both water-wet and oil-wet pores. Furthermore, during oil flooding, we observed minimal variation in the area of the NMR T_2 spectrum, which indicates that water production is negligible throughout this process.Fig. 4The NMR T2 spectral during the amott wettability index tests.Fig. 4The NMR T2 spectral during the amott wettability index tests.Fig. 4The NMR T2 spectral during the amott wettability index tests.

NMR T_2 spectrum during the imbibition test sample

Figure 5 show the NMR T_2 spectrum curve at the difference imbibition time and injection pressure. In all sample, the oil-saturated (i.e. irreducible water) spectrum were weakly bimodal, with main peak at relaxation time between 10 and 1000 ms. With the increase of imbibition time, the area of the T_2 spectrum of the sample gradually decreases, and there are significant differences in the variation characteristics of the nuclear magnetic resonance T_2 spectrum under different injection pressures. When the injection pressure is 0 MPa (the fluid relies entirely on the capillary pressure of the rock for oil recovery), the changes in the T_2 spectrum are mainly reflected in the part with a relaxation time greater than 10 ms, while the changes in the nuclear magnetic resonance T_2 spectrum within a relaxation time less than 10 ms are not significant (Fig. 5). As the injection pressure gradually increases, the signals amplitude of T_2 spectrum with relaxation times greater than 20 ms and less than 5 ms decreases with the increase of imbibition time, while the signal amplitude corresponding to relaxation times of 5–20 ms fluctuates up and down in a range (Fig. 5).

Discussion
The wettability of the samples in the difference pore-throat space

Based on the variation in the T_2 spectrum during the Amott tests, the recovery factor was determined using the following formula during spontaneous imbibition water or oil, respectively.

$$E_{ws-ri} = \frac{\int_{r_{i\min}}^{r_{i\max}} m\,(r_i)_{bw}\,dr_i - \int_{r_{i\min}}^{r_{i\max}} m\,(r_i)_{aw}\,dr_i}{\int_{r_{\min}}^{r_{\max}} m\,(r_i)_{bw}\,dr_i} \tag{7}$$
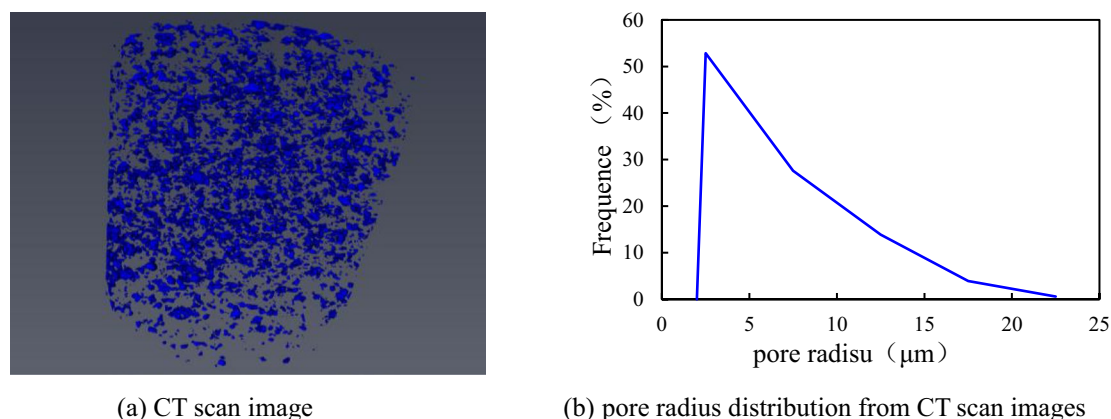

(a) CT scan image   (b) pore radius distribution from CT scan images

Fig. 3. CT scan image and pore throat distribution.

(a) Sample of 1#

(b) Sample of 2#

(c) Sample of 3#
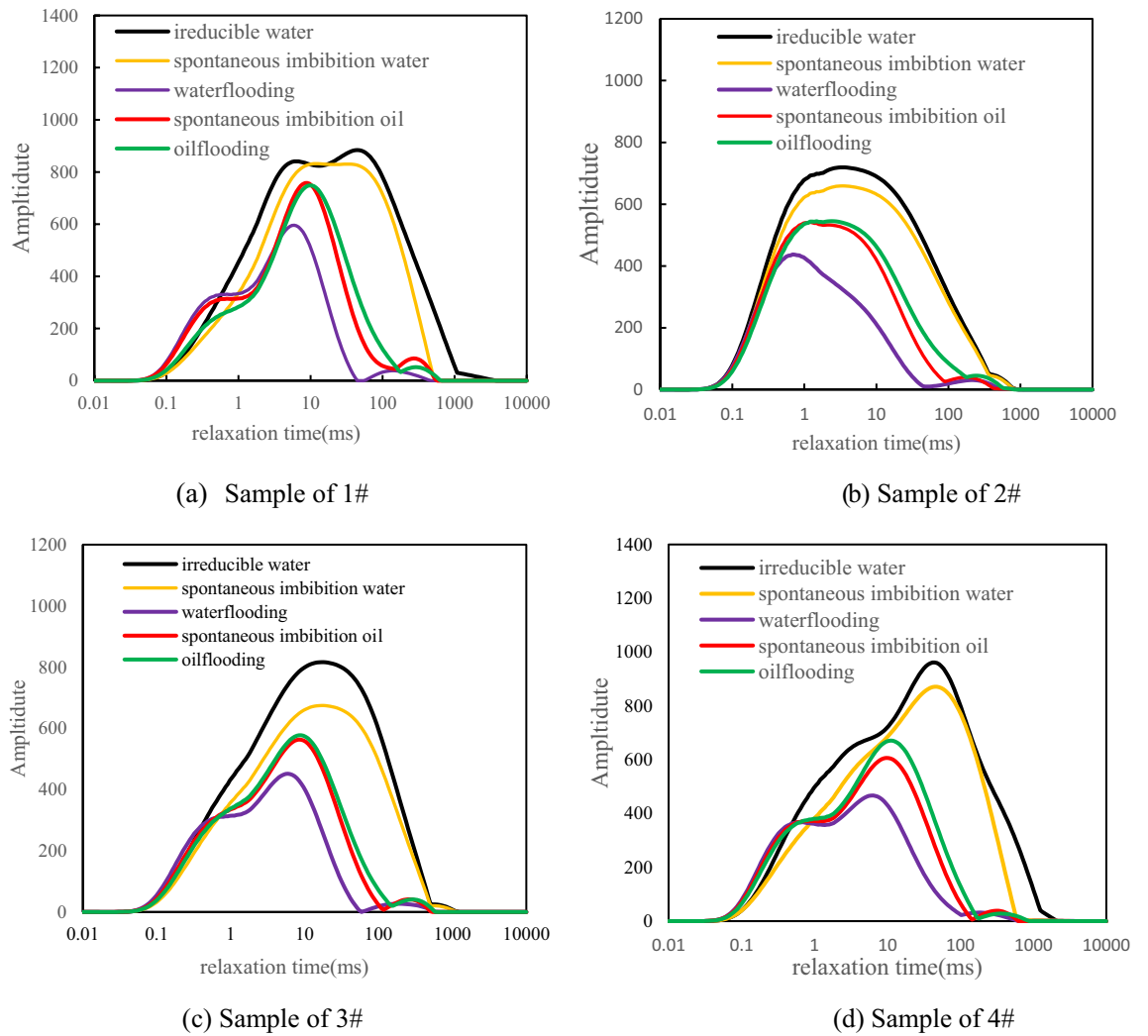

(d) Sample of 4#

Fig. 4. The NMR T_2 spectral during the amott wettability index tests.

$$E_{os-ri} = \frac{\int_{r_{i\,\min}}^{r_{i\,\max}} m\,(r_i)_{ao}\,dr_i - \int_{r_{i\,\min}}^{r_{i\,\max}} m\,(r_i)_{bo}\,dr_i}{\int_{r_{\min}}^{r_{\max}} m\,(r_i)_{ao}\,dr_i} \tag{8}$$

where $E_{ws\text{-}ri}$ is the recovery factor of the sample during spontaneous imbibition water; $E_{os\text{-}ri}$ is the recovery factor of the sample during spontaneous imbibition oil; $m(r_i)_{bw}$ and $m(r_i)_{aw}$ are the T_2 amplitudes before and after spontaneous imbibition water (A/m), respectively; $m(r_i)_{bo}$ and $m(r_i)_{ao}$ are the T_2 amplitudes before and after spontaneous imbibition oil (A/m), respectively;

Similarly, the oil recovery factor was calculated during waterflooding or oilflooding using the following formula:

$$E_{wd-rj} = \frac{\int_{r_{j\,\min}}^{r_{j\,\max}} m\,(r_j)_{bd}\,dr_j - \int_{r_{j\,\min}}^{r_{j\,\max}} m\,(r_j)_{ad}\,dr_j}{\int_{r_{\min}}^{r_{\max}} m\,(r_j)_{b}\,dr_j} \tag{9}$$

$$E_{od-rj} = \frac{\int_{r_{j\,\min}}^{r_{j\,\max}} m\,(r_j)_{ad}\,dr_j - \int_{r_{j\,\min}}^{r_{j\,\max}} m\,(r_j)_{bd}\,dr_j}{\int_{r_{\min}}^{r_{\max}} m\,(r_j)_{a}\,dr_j} \tag{10}$$

where $E_{wd\text{-}rj}$ is the recovery factor of the sample during waterflooding; $E_{od\text{-}rj}$ is the recovery factor of the sample during oilflooding; $m(r_i)_{bd}$ and $m(r_i)_{ad}$ are the T_2 amplitudes before and after waterflooding (A/m), respectively; $m(r_i)_{ad}$ and $m(r_i)_{bd}$ are the T_2 amplitudes before and after oilflooding (A/m), respectively. According to definitions of the water wettability index and water wettability index, we can calculate these indices for difference pore-throat based on the recovery factor (Eq. 7 - 10), and determine the proportions of oil-wet and water-wet pores within the sample.

(a) Sample of 1#

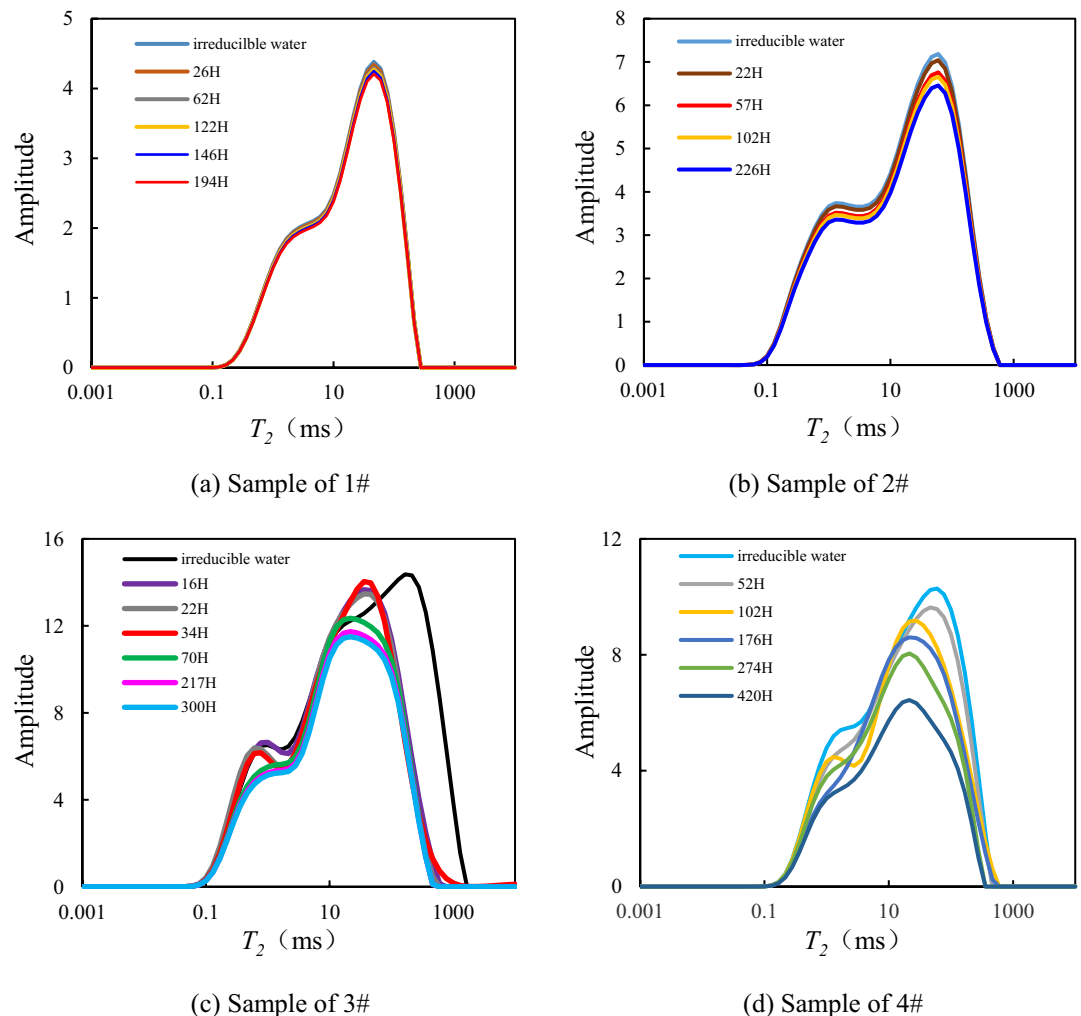(b) Sample of 2#

(c) Sample of 3#

(d) Sample of 4#

Fig. 5. NMR spectra of rock samples during dynamic imbibition process.

Figure 6 illustrates the wettability variations across different pore-size domains within the sample matrix. A notable finding was the distinct wettability differentiation among pore-size classifications. Microscopic analysis revealed that microporous regions (pore radius < 0.1 μm) exhibited strongly water-wet characteristics, with water wettability indices approaching 1. Conversely, mesoporous domains (0.1–3 μm radius range) demonstrated progressive oil-wet predominance, showing an inverse correlation between pore size and water wettability. Macropores (> 3 μm) reverted to water-wet behavior, with oil wettability indices decreasing by 62.4% compared to mesopores. Table 2 presents statistical data on the proportion of water-wet pores versus oil-wet pores within micropores, mesopores, and macropores across all samples. On average, it was found that 43.25% exhibit water-wet characteristics while 56.75% display oil-wet characteristics overall. Specifically, micropores and macropores show relatively high proportions of water-wet pores at averages of 14.57% and 26.94%, respectively; conversely, mesopores exhibit a markedly lower average proportion at only 1.94%. In contrast to other pore size categories, mesopores have the highest average proportion (36.96%) of oil-wet pores.

The effect of the displacement pressure on migration of fluid during the imbibition

Based on the classification of pore throat space, we also conducted an estimation of oil recovery in three different pore classes and total oil recovery under varying pressure conditions during the force imbibition process based on the variation of the NMR T_2. The relationship between oil recovery and imbibition time was plotted (Fig. 7). Our findings revealed significant differences in the oil flow characteristics of shale oil under different injection pressures during the force imbibition process. In instances where there is no pressure difference between the matrix and fractures (i.e., when injection pressure is 0 MPa, and the rock relies solely on capillary pressure for spontaneous imbibition), it was observed that oil mainly originates from macropores (Fig. 7a). The contribution of macropore oil recovery (approximately 25% of large pores in the rock sample) to total oil recovery was as high as 62.08% (Fig. 7a). Conversely, crude oil recovery degree in mesopores and micropores was minimal, with their combined contribution to total infiltration recovery degree amounting to only 38.92% (Fig. 7a), consistent with wettability characteristics of the rock sample. The samples exhibited hydrophilic characteristics within their macropores, with capillary pressure serving as a driving force during imbibition. Additionally, connectivity
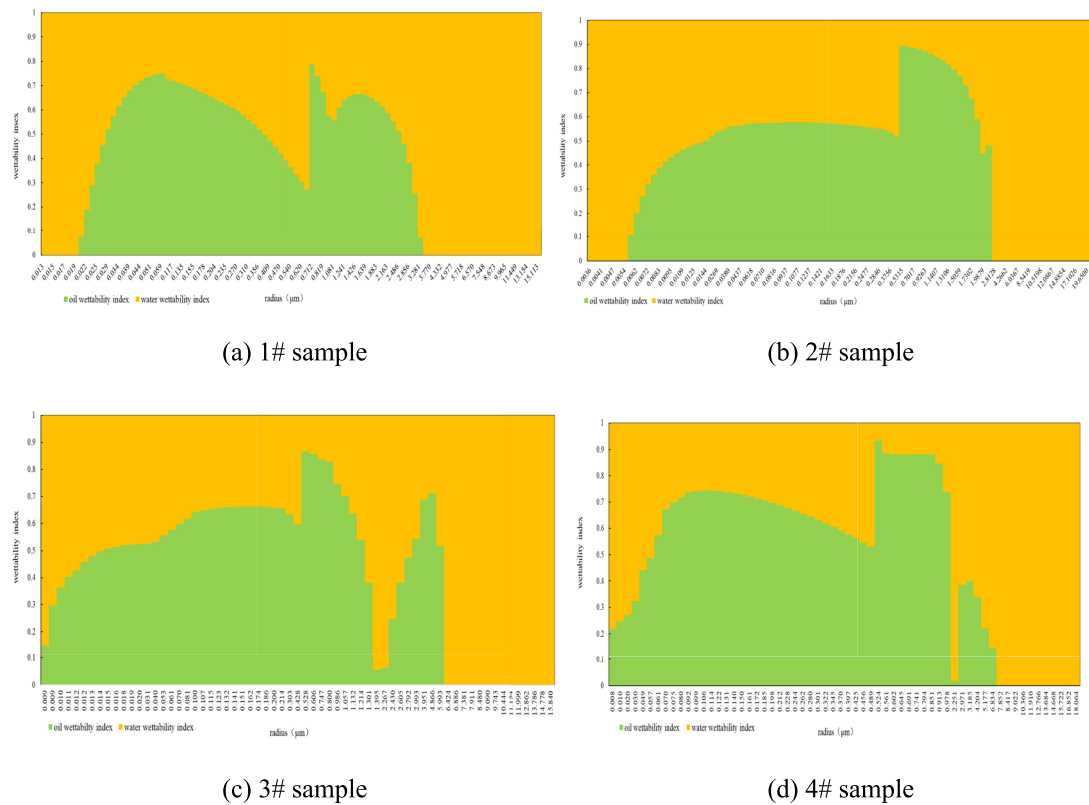
(a) 1# sample

(b) 2# sample

(c) 3# sample

(d) 4# sample

Fig. 6. The wettability characteristics in the difference pore space of sample.

Sample	Micropore		Mesopore		Macropore		Water wet pore (%)	Oil wet pore(%)
	Water wet (%)	Oil wet(%)	Water wet (%)	Oil wet(%)	Water wet (%)	Oil wet(%)		
1#	12.30	4.61	0	46.15	30.76	6.15	43.10	56.90
2#	13.33	12.22	7.77	26.67	27.77	12.22	48.00	52.00
3#	22.98	9.19	0	37.93	21.83	8.04	44.80	55.20
4#	9.67	9.67	0	37.09	27.41	16.12	37.10	62.90
average	14.57	8.92	1.94	36.96	26.94	10.63	43.25	56.75

Table 2. The wettability characters in the difference pore.

among macropores was relatively strong, resulting in effective crude oil production through capillary imbibition. When a pressure difference exists between the matrix and fracture (i.e., when injection pressure is not at zero), overall flow characteristics of oil can be divided into two stages. In the initial stage, the fracturing fluid penetrates the larger pores surrounding the fracture due to the pressure differential between the matrix and the fracture. This results in a rapid increase in recovery within these larger pores (see Fig. 8), with potential recovery rates reaching as high as 25% (see Fig. 8). In the subsequent stage, as the pressure differential between the matrix and fractures diminishes during pressure transmission, water retained within macropores and fractures undergoes spontaneous imbibition into micropores along particle surfaces. This process occurs under dual influences of capillary forces and displacement pressure differentials (see Fig. 7b, c, and d), leading to an increased oil recovery from micropores of up to 5% (see Fig. 8).

By comparing the oil recovery under different pressure differences, we found that the existence of pressure difference will be conducive to improving the oil–water imbition effect during the shut-in process. We can further substantiate this perspective through a simplified capillary bundle model combined with numerical calculations. Assuming the presence of two phases—oil and water—in a single capillary tube with radius (r), the displacement pressure and capillary forces are regarded as the driving forces, while the viscous resistance between oil and water, as well as against the pore throat wall, is considered as an opposing force. The interface between the oil–water phases at time (t) can thus be described as follows[31–34]::
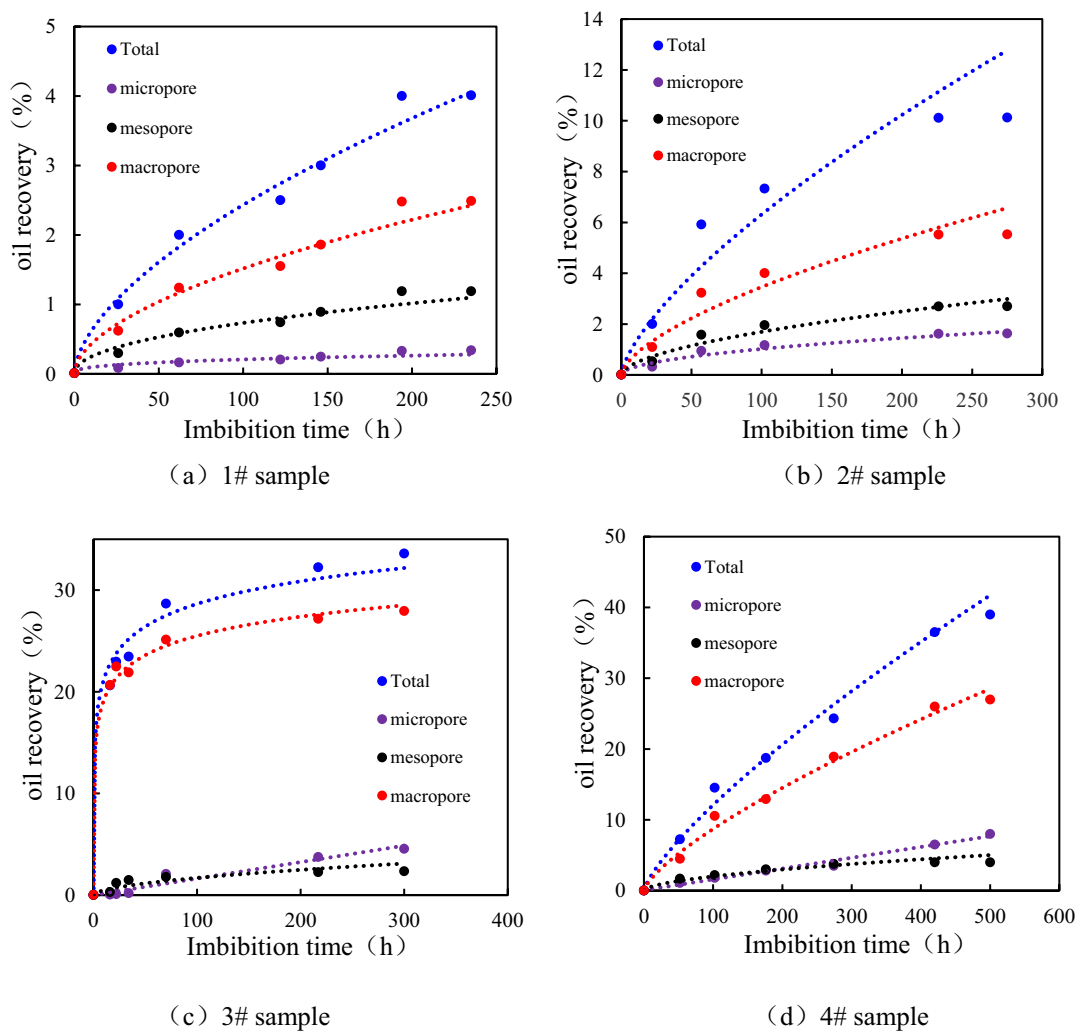
Fig. 7. Dynamic imbibition characteristics of rock samples in different pore throat spaces.
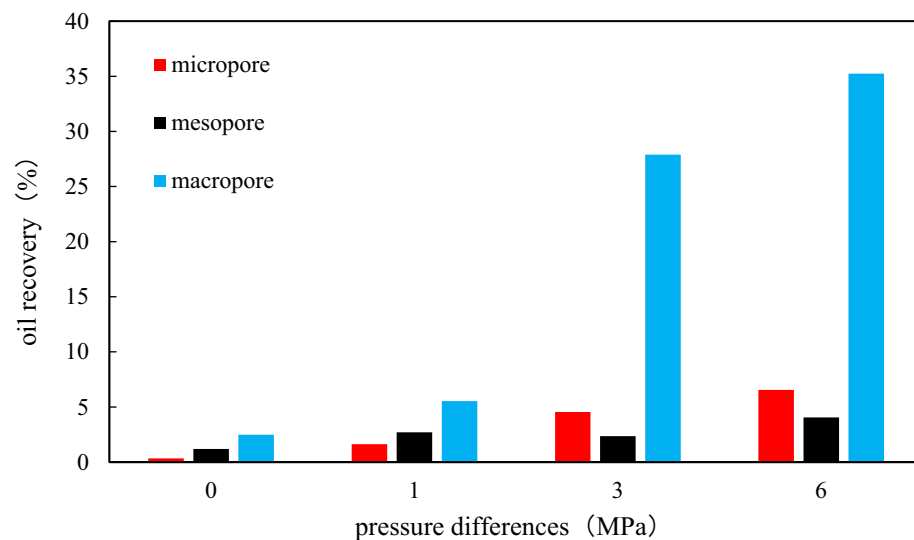

Fig. 8. The variation characteristics of oil recovery under different pressures different.

$$x = \frac{L}{1 - \frac{\mu_w}{\mu_o}} - \frac{\sqrt{L^2 - \frac{r^2}{4\mu_o}\left(1 - \frac{\mu_w}{\mu_o}\right)\left(\Delta p + \frac{2\sigma\cos\theta}{r}\right)t}}{1 - \frac{\mu_w}{\mu_o}} \qquad (11)$$

where Δp represents the pressure difference (MPa); σ represents the interfacial tension (mN/m); θ is the contact angle (°); r is the capillary tube radius (μm); v_d is the fluid flow velocity of the displacemnt (μm³/s); μ_o and μ_d represent the viscosities of oil and displacement fluid (mPa·s), respectively; L is the length of the capillary tube (μm); and x is the location of the oil–water interface. Assuming that $\mu_w = 1$ mPa·s, $\mu_g = 0.018$ mPa·s, $\mu_o = 1.3$ mPa·s, $\sigma_{og} = 72$ Nm/m, $\sigma_{ow} = 25$ Nm/m, $L \approx 450$ μm, $\theta = 75°$, the location of the oil–water interface in the tube using different pressure difference can be calculated by solving the Eq. (11). We observed that when the displacement pressure gradient is 0 MPa/m (i.e., the oil–water imbibition displacement is completely dependent on capillary pressure), the time for the oil–water interface to reach the capillary outlet is 2200 s (Fig. 9). As the displacement pressure increases, the time for the oil–water interface to reach the capillary outlet gradually shortens. When the displacement pressure gradient is 2 MPa/m, the time for the oil–water interface to reach the capillary outlet is only 1040 s (Fig. 9). This means that the presence of a pressure difference facilitates the propulsion distance of fracturing fluid during shut-in. In contrast, without a pressure difference (i.e., spontaneous imbibition), the action range and efficacy of fracturing fluid are limited to hydrophilic larger pores. Capillary imbibition, on the other hand, induces displacement of the propulsion front, reducing water saturation within the wave range of fracturing fluid and enabling penetration into smaller pores and throats. This displaces formation fluid and enhances imbibition displacement effects. Therefore, increasing the pressure difference between the fracture and matrix can enhance oil recovery during shut-in and alter the range of oil distribution for imbibition.

The relationship between the optimal shut-in time and displacement pressure

We have discovered that the pressure differential between the matrix and fractures during imbibition can significantly enhance oil recovery, as demonstrated by our experimental findings. However, it has proven challenging to quantitatively establish the relationship between optimal shut-in time and displacement pressure across different types of shale oil reservoirs through experiments alone. Consequently, we have undertaken numerical simulations of"shut-in"using reservoir numerical simulation with COMSOL Multiphysics. The model simplifies the complex network of fractures resulting from volumetric fracturing into a combination of horizontal wells, artificial fractures (main fractures), and matrix systems (Fig. 10). Within this model grid, horizontal wells are positioned at the center of artificial fractures. These artificial fractures are symmetrically arranged within the vertical fractures associated with the horizontal wells and characterized by parameters such as fracture length, width, and height. The matrix system is uniformly distributed around these artificial fractures; its reservoir characteristics and percolation capabilities are dictated by porosity and permeability. In accordance with the reservoir characteristics in the study area, we designed three types of models. Type I reservoirs, micro-fractures are well developed and the reservoir physical properties are good. The permeability of matrix systems is set at 3 mD; Type II reservoirs, local micro-fractures are well developed and the reservoir physical properties are relatively good. The permeability of matrix systems is set at 1 mD; Type II reservoirs, the micro-fractures are underdeveloped. The reservoirs are mainly composed of matrix pores, with low physical properties. The permeability of matrix systems is set at 0.1 mD. Besides, the foundational data utilized in this model is derived from reservoir data specific to our study area (Table 3).

Figure 11–13 illustrate the distribution of formation pressure during the imbibition of fracturing fluid. From these figures, it is evident that the characteristics of pressure wave changes during the shut-in process are fundamentally similar across all three types of reservoirs. As shut-in pressure increases, the coverage area of the pressure wave progressively expands. In Type I reservoirs, superior reservoir physical properties lead to enhanced connectivity between pores and throats, resulting in reduced flow resistance between oil and water.
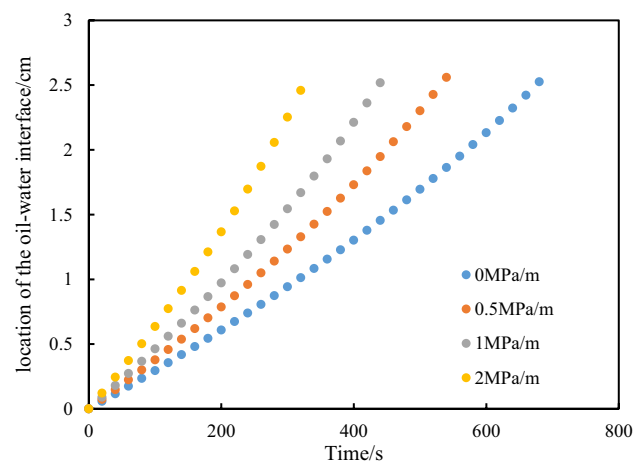

Fig. 9. The variation of the position of the oil–water interface in the capillary over time.
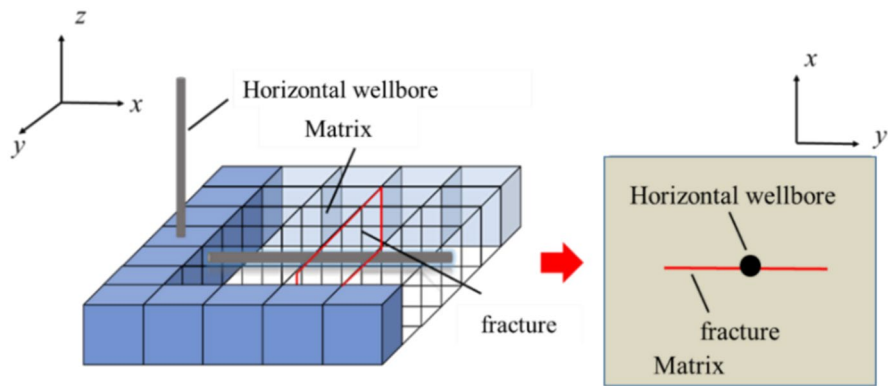
Fig. 10. Schematic diagram of the physical model.

No	Parameter	Value	No	Parameter	Value
1	Matrix porosity(%)	8	7	Fracture width(m)	0.007
2	The permeability of matrix systems(mD)	0.1、1、3	8	Half-length fracture(m)	150
4	Initial formation pressure(MPa)	20	9	Fracture permeability(D)	1
5	Crude oil viscosity(mPa·s)	1.5	10	Oil density(kg/m^3)	850
6	Water phase density(kg/m^3)	1000	11	Water phase viscosity(mPa·s)	1

Table 3. Basic physical property parameters required in simulation program.

(a)35MPa (b)45MPa (c)55MPa (d)65MPa
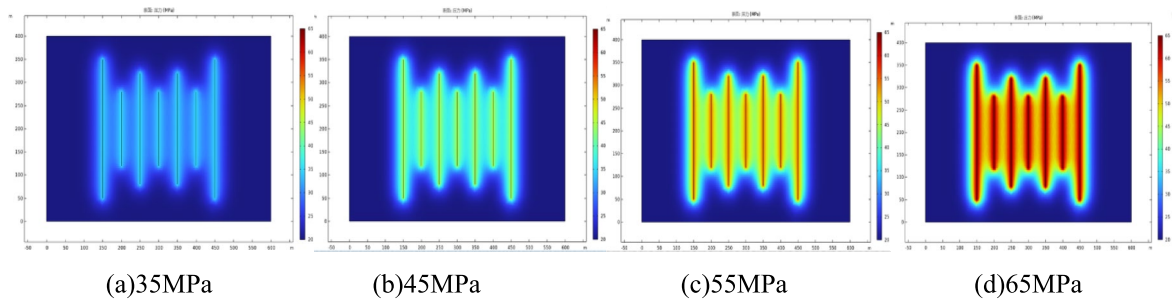
Fig. 11. Fracturing fluid conduction distribution at the difference shut-in pressure for I type reservoir.

(a)35MPa (b)45MPa (c)55MPa (d)65MPa
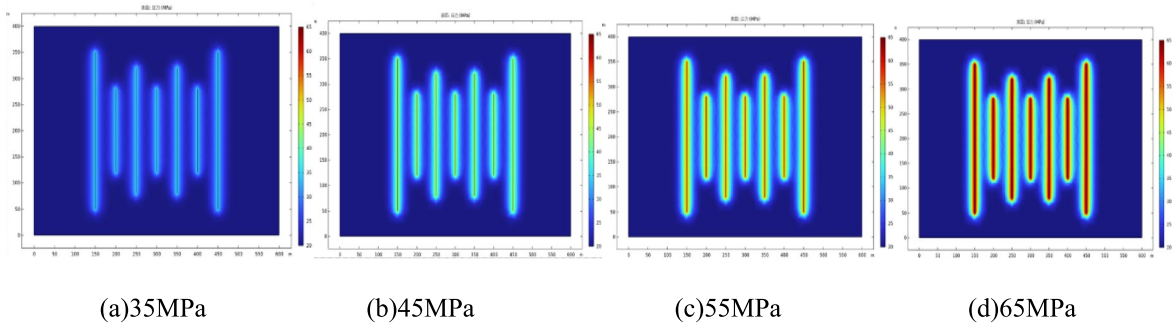
Fig. 12. Fracturing fluid conduction distribution at the difference shut-in pressure for II type reservoir.

Consequently, achieving a balanced state in oil–water flow becomes more feasible. Therefore, with higher shut-in pressures, there is a more pronounced effect on increasing formation energy and an enlarged spreading area during imbibition. We further analyze the variation characteristics of imbibition distance among the three types of reservoirs (Fig. 14). Our findings reveal that at low pressures, variations in imbibition distance across
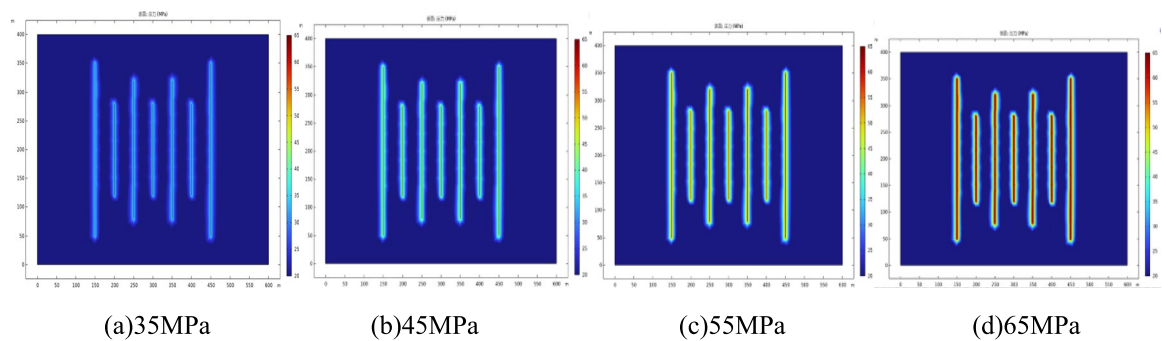
(a)35MPa   (b)45MPa   (c)55MPa   (d)65MPa

Fig. 13. Fracturing fluid conduction distribution at the difference shut-in pressure for III type reservoir.
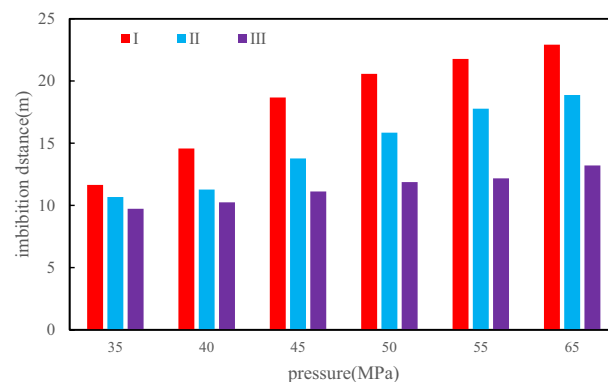

Fig. 14. The variation of the imbibition distance at the difference pressure for three type reservoir.

these reservoir types are minimal—within a mere range of 1.92 m. However, as pressure escalates, disparities in imbibition distance among these reservoir types become increasingly pronounced. For Type I reservoirs, significant variation in imbibition distance occurs with changes in pressure; specifically, when pressure rises from 35 to 65 MPa, imbibition distance doubles. Notably, this increase begins to diminish when pressures exceed 45 MPa. In Type II reservoirs, a gradual decrease in increment for imbibition distance is observed once pressures surpass 55 MPa. Conversely, for Type III reservoirs, variations in imbibition distance show little correlation with changes in pressure; from 35 to 65 MPa increments only yield an increase by a factor of 1.35 times. At this stage for Type III reservoirs, fracturing fluid predominantly flows along fractures while its spreading area remains limited during immersion (Fig. 14).

The time point at which the imbibition distance remains relatively constant is regarded as the optimal shut-in time under specific pressure conditions. We further analyzed the variations in pressure and optimal shut-in time across different types of reservoirs (Fig. 15). Our findings indicate that the optimal shut-in time gradually decreases with increasing pressure, with the most pronounced changes observed in type I and II reservoirs. Additionally, when the pressure surpasses a certain threshold, the optimal shut-in time exhibits minimal variation despite further increases in pressure. For type I reservoirs, when the pressure is below 50 MPa, there is significant variability in shut-in times corresponding to increases in pressure—ranging from 40 days down to 23 days. However, once the pressure exceeds 50 MPa, changes in shut-in times become negligible. This suggests that beyond this point, the imbibition distance of fracturing fluid does not alter significantly; consequently, oil–water imbibition exchanges achieve near-optimal effectiveness for type I reservoirs at pressures greater than 50 MPa. At this stage, continued increases in pressure will primarily extend drilling duration without substantially enhancing imbibition recovery. Therefore, we recommend maintaining a reasonable shut-in pressure for type I reservoirs at approximately 50 MPa, with an associated recommended shut-in time of around 20 days. Similarly, for Type II reservoirs, when the pressure exceeds 55 MPa, the shut-in time remains relatively constant. Thus, a reasonable shut-in pressure for Type II reservoirs is determined to be 55 MPa, with an associated shut-in duration of approximately 30 days. In contrast, for Type III reservoirs, the variation in shut-in time relative to pressure is minimal. When pressure increases from 35 to 65 MPa, the change in shut-in time is only about five days. This indicates that for this type of reservoir, an increase in pressure offers limited enhancement to imbibition recovery; consequently, the overall spread area of fracturing fluid is restricted (primarily propagating around the fracture as shown in Fig. 13), and there is a high degree of pressure retention overall. Therefore, we recommend maintaining as high a pressure as possible for Type III reservoirs in order to minimize shutdown duration and reduce ineffective shut-in.
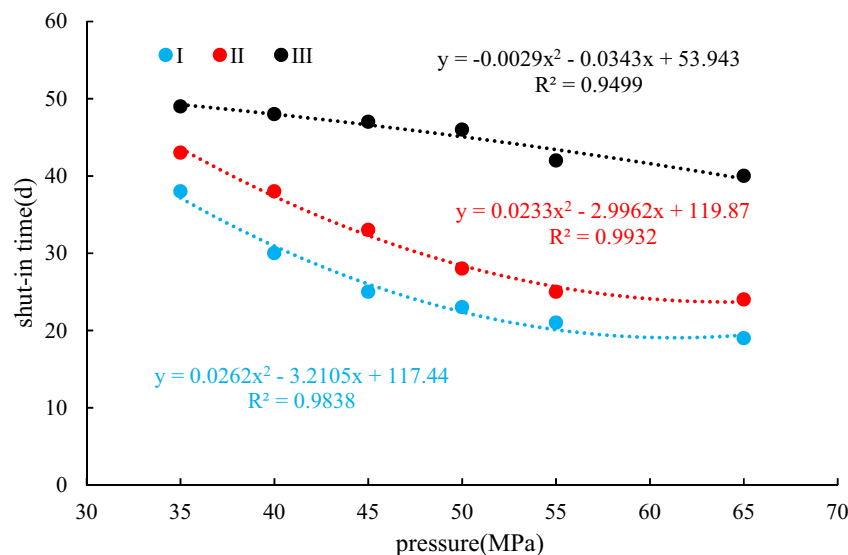
Fig. 15. The variation of the pressure and shut-in time.

Conclusion

(1) The sample of tight exhibit the mix-wettability, and the micropores and macropores exhibit strong water wetting characteristics, while mesopores demonstrate relatively strong oil wetting characteristics.

(2) During the process of "shut-in" after the hydraulic fracturing at the difference shut-in pressure, the fracturing fluid can be divided into the two stage. The fracturing fluid first mobilizes the crude oil in macropores under the combined action of pressure difference and capillary pressure, with a recovery rate of up to 25%. Then its infiltration evolves into a spontaneous imbibition process, resulting in a lower recovery rate mainly from micropores.

(3) Increasing the pressure difference between the fracture and matrix can enhance oil recovery for reservoirs with the higher reservoir permeability, and the reasonable shut-in pressure is 45 MPa ~ 55 MPa, the corresponding shut-in time is about 20 ~ 30 days. For the reservoir, with low physical properties, an increase in pressure offers limited enhancement to imbibition recovery.

Data availability

The full raw data from this study cannot be publicly shared due to the potential risk of identifying or exposing sensitive patient information. However, selected datasets used in the study may be available upon request from the corresponding author, subject to meeting the criteria for access to confidential data.

References

1. Zou, C. N. et al. Formation mechanism, geological characteristics and development strategy of nonmarine shale oil in China. *Pet. Explor. Dev.* **40**(1), 14–26. https://doi.org/10.1016/S1876-3804(13)60002-6 (2013).
2. Jia, C. Z., Zheng, M. & Zhang, Y. F. Unconventional hydrocarbon resources in China and the prospect of exploration and development. *Pet. Explor. Dev.* **39**(2), 129–136 (2012).
3. Jing, Z. J. et al. Research progress and key scientific issues of continental shale oil in China. *Acta petrolei sinica* **42**(07), 821–835 (2021).
4. Hu, S. Y. et al. Development potential and technical strategy of continental shale oil in China. *Pet. Explor. Dev.* **47**(04), 819–828 (2020).
5. Lei, Q., Wen, D.W., Guan, B.S., *et al.* Shale oil and gas exploitation in China: Technical comparison with US and development suggestions. *Petroleum exploration and development* 2023 1–8.
6. Zhang, L. H. et al. Advancements in shale oil/gas research in north american and considerations on exploration for lacustrine shale oil/gas in China. *Adv. Earth Sci.* **29**(06), 700–711 (2014).
7. Hou, L.H., W, S.T., Jiang, X.H., *et al.* Situation, challenge and future direction of experimental methods for geological evaluation of shale oil. *Acta petrolei sinica*, 2023, 44(01): 72–90.
8. Fu, S. T. et al. Accumulation conditions and key exploration and development technologies in Q ingcheng oilfield. *Acta petrolei sinica* **41**(07), 777–795 (2020).
9. Wang, Q. et al. Shut-in time optimization after fracturing in shale oil reservoirs. *Pet. Explor. Dev.* **49**(03), 586–596 (2022).
10. Wang, Z. N. et al. Evaluation of pore-scale wettability in the tight sandstone reservoirs of the upper triassic yanchang formation, ordos basin, China[J]. *Mar. Pet. Geol.* **138**, 105528 (2022).
11. Cheng, Y. Impact of water dynamics in fractures on the performance of hydraulically fractured well sing as-shale reservoirs. *J. Can. Pet. Technol.* **51**(2), 143–151 (2012).
12. Fakcharoenphol, P. et al. Effect of shut-in time on gas flow rate in hydraulic fractured shale reservoirs. *J. Nat. Gas Sci. & Eng.* **32**, 109–121 (2016).

13. N, Bostrom., M, Chertov., M, Pagels. The time-dependent permeability damage caused by fracture fluid. SPE international symposium and exhibition on formation damage control, Lafayette, Louisiana, USA, February 2014.
14. Dutta, R. et al. Experimental investigation of fracturing-fluid migration caused by spontaneous imbibition in fractured low-permeability sands. *SPE Res. Eval. & Eng.* **17**, 74–81 (2014).
15. Wang, X. et al. Characteristics of oil distribution in forced and spontaneous imbibition of tight oil reservoir. *Fuel* **221**, 280–288 (2018).
16. Guo, Q. X. et al. Characteristics and influencing factors for forced imbibition in tight sandstone based on Low-field nuclear magnetic resonance measurements. *Energy & fuel* **32**, 8230–8240 (2018).
17. Wang, F. et al. A pressure drop model of post-fracturing shut-in considering the effect of fracturing-fluid imbibition and oil replacement. *Pet. Explor. Dev.* **48**(06), 1250–1257 (2021).
18. Yaich E. Williams S, Bowser A. et al. A case study. The impact of soaking on well performance in the Marcellus. URTEC 2154766-MS19 2015.
19. Yang, P., Hekun, G. & Daoyong, Y. Determination of residual oil distribution during waterflooding in tight oil formation with NMR relaxometry measurements. *Energy Fuels* **27**, 5750–5756 (2013).
20. Wei, Q. et al. An experimental study on the effect of microscopic pore structure on spontaneous imbibition in tight sandstones. *Pet. Drill. Tech.* **44**(05), 109–116 (2016).
21. Lai, F. P. et al. Experimental investigation of spontaneous imbibition in tight reservoir with nuclear magnetic resonance testing. *Energy Fuels* **30**(11), 8932–8940 (2016).
22. Yang, Y.B., Xiao, W.L., Zheng, L.L., et al. Pore throat structure heterogeneity and its effect on gas-phase seepage capacity in tight sandstone reservoirs: A case study from the Triassic Yanchang Formation, Ordos Basin. Petroleum Science,2023.
23. Chen, M. et al. Differences in the fluid characteristics between spontaneous imbibition and drainage in the tight sandstone cores from nuclear magnetic resonance. *Energy Fuels* **32**(10), 10333–10343 (2018).
24. Nie, R. S., Zhou, J, Chen, Z. X., Liu, J. C. & Pan, Y. Pore structure characterization of tight sandstones via a novel integrated method: A case study of the Sulige gas field, Ordos Basin (Northern China). *J. Asian Earth Sci.* **213**, 104739 (2021).
25. Xiao, W. L. et al. Experimental study on the oil production characteristics during the waterflooding of different types of reservoirs in ordos Basin. *NW China. Pet. Explor. & Dev.* **48**(4), 807–816 (2021).
26. Xiao, W. L. et al. Rock wettability and its influence on crude oil producing characteristics based on the NMR technology. *Pet. Geol. & Recover. Effic.* **30**(1), 112–121 (2023).
27. Yang, Y. B. et al. Effect of pore structure and injection pressure on waterflooding in tight oil sandstone cores using NMR technique and pore network simulation. *J. Petrol. Sci. Eng.* **217**, 110886 (2022).
28. Alhammadi, A. M. et al. In situ characterization of mixed-wettability in a reservoir rock at subsurface conditions. *Sci. Rep.* **7**(1), 1–9 (2017).
29. Singh, K., Bijeljic, B. & Blunt, M. J. Imaging of oil layers, curvature and contact angle in a mixed-wet and a water-wet carbonate rock. *Water Resour. Res.* **52**(3), 1716–1728 (2016).
30. Gerald, K. E. et al. The effect of wettability on waterfood oil recovery in carbonate rock samples: A systematic multi-scale experimental investigation. *Transp. Porous Media* **138**(2), 369–400 (2021).
31. Wang, F. Y., Zeng, F. C. & Zhao, J. Y. A mathematical model of displacement and imbibition of low-permeability/tight reservoirs and its application. *Acta Petrolei Sinica* **41**(11), 1396–1405 (2020).
32. Wang, F. Y. & Zhao, J. Y. A mathematical model for co-current spontaneous water imbibition into oil-saturated tight sandstone: Upscaling from pore-scale to core-scale with fractal approach. *J. Petrol. Sci. Eng.* **178**, 376–388 (2019).
33. Wu, Y. et al. An approximate semi analytical method for two-phase flow analysis of liquid rich shale gas and tight light-oil wells. *J. Petrol. Sci. Eng.* **176**, 562–572 (2019).
34. Li, W. et al. Large-scale gas accumulation mechanisms and reservoir-forming geological effects in sandstones of Central and Western China. *Pet. Explor. Dev.* **47**(4), 714–725 (2020).

Author contributions
"Yang Y.B., Peng X., Xiao W.L. wrote the main manuscript text and Lei Q.H., He Y.A., Zheng L.L prepared data. All authors reviewed the manuscript.

Funding

Declarations

Competing interests
The authors declare no competing interests.

Additional information
Supplementary Information The online version contains supplementary material available at https://doi.org/10.1038/s41598-025-07636-9.

Correspondence and requests for materials should be addressed to W.X.

Reprints and permissions information is available at www.nature.com/reprints.

Publisher's note Springer Nature remains neutral with regard to jurisdictional claims in published maps and institutional affiliations.